Colloid Polym Sci (2008) 286:603–609
DOI 10.1007/s00396-008-1838-6

SHORT COMMUNICATION

Effect of the acrylic acid content on the permeability and water uptake of poly(styrene-co-butyl acrylate) latex films

Yuri Reyes-Mercado · Flavio Vázquez · Francisco J. Rodríguez-Gómez · Yurko Duda

Received: 23 November 2007 / Accepted: 9 January 2008 / Published online: 6 February 2008

Abstract In this contribution, a theoretical modeling of the latex film formation is presented and compared to experimental results: water vapor permeability and latex film capacitance are studied as a function of acrylic acid content in poly(styrene-*co*-butyl acrylate) latex films. It has been shown that both water uptake and water vapor permeability are mainly affected by film morphology which in turn is defined by intercolloidal interaction and drying rate.

Keywords Latex film · Acrylic acid · Drying · Simulation

Introduction

Latexes are aqueous dispersions of polymeric particles that may be employed to produce coatings, paints, adhesives, etc. [1, 2]. It has been pointed out that the use of latex will grow beyond the current uses because of their low or null environmental impact, since these systems employ water as dispersive medium [3, 4].

Latexes are commonly obtained by emulsion polymerization reactions. In this polymerization technique, a monomer, or a mixture of them are emulsified in water by means of a surfactant. In order to ensure an adequate reaction rate, it is common to introduce an initiator to the reaction system. The surfactant influences the nucleation of polymer particles, the particle size distribution, and the colloidal stability of the latex as well as the film properties [5]. Another method commonly used to confer colloidal stability to a dispersed polymer is to place electrostatic charges on the particle surface; this is done by adding a small amount of functional monomers such as acrylic or methacrylic acid over the particle surface [6]. In addition, this monomer can promote the adhesion of the film to the substrate, which is of primary importance in polymer coatings [7].

In order to obtain high performance coatings, not only the nature of the polymer must be taken into account. The experimental conditions such as temperature, humidity, drying rate, and characteristics of the substrate play an important role in the film formation process [8]. Although latex films are widely used and extensively studied nowadays, the exact mechanism involved in the transformation of a polymer dispersion into a coherent polymer film is not well established and several aspects of the process remain insufficiently understood [9–12]. Usually, the film formation process is divided in three stages: (1) evaporation of water resulting in packing of latex particles, (2) their deformation, and (3) coalescence by interdiffusion of polymer chains between adjacent particles. The first stage is crucial because the structure achieved by the particles will remain in the film, affecting the subsequent stages and final film properties [13, 14]. If the particles have enough time to pack, i.e., low evaporation rate of water, a dense packing could be obtained [15]. However, since the surface electrostatic charges of the polymer particles modify the interaction among them, the packing of the polymer particles is affected by changing the amount of functional monomer.

The permeability and water uptake of the latex film affect its performance. When in contact with water, the

Y. Reyes-Mercado · F. J. Rodríguez-Gómez
Facultad de Química, UNAM,
04510 México, México

Y. Reyes-Mercado (✉) · F. Vázquez · Y. Duda
Programa de Ingeniería Molecular,
Instituto Mexicano del Petróleo,
07730 México, México
e-mail: yurirm@lycos.com

coating tends to absorb water, swells, and often the adhesion is lost or decreased [16]. Besides, small hydrophilic molecules such as surfactants employed in the polymerization reaction, pigments, or water-soluble oligomers, can be extracted from the film by water, which provokes the loss of film properties [17]. In addition, the measurement of latex film permeability may help to infer the internal film morphology [18].

The aim of the present work is to analyze the effect of the amount of a functional monomer, AA, on the poly (styrene-*co*-butyl acrylate) latex film applying computer simulation and experimental techniques.

Experimental

The monomers, *n*-butyl acrylate (BuA), methyl methacrylate (MMA), styrene (S), and acrylic acid (AA) technical grade were purchased from Celanese S.A (Mexico). Ammonium persulfate (Fermont) and sodium bicarbonate (J.T. Baker) were used as initiator and buffer, respectively. Two surfactants, Abex 26 S® (Sodium salt of an ethoxylated sulfated alkyl phenol) from Rhodia and Disponil ALS 28® (Ammonium lauryl sulfate) from Cognis were used without further purification. Distilled water was used during the experiments and all reactants were used as received.

The polymerization formulation is shown in Table 1. The amount of BuA/MMA ratio was kept constant; however, as AA was introduced in the formulation, the same quantity of S was removed, i.e., 98.4 g of S and 9.6 g of AA were used to prepare the copolymer with 4% of AA and so on. The amount of AA used in this study was 2, 4 and 6 wt.% of the monomer phase. Since AA and its polymer are water-soluble, most of this component would be located at the particle surface instead of going into the core of the polymer particle, mainly composed of hydrophobic monomers [19, 20].

Table 1 Composition of the polymerization formulation employed in the synthesis of emulsion copolymers with different amount of acrylic acid

Substance	Main reactor (g)	Feeding tank (g)
n-Butyl acrylate	0	120
Methyl methacrylate	0	12
Styrene	0	103.2, 98.4 and 93.6
Acrylic acid	0	4.8, 9.6 and 14.4
Ammonium persulfate solution 5 wt.%	26	70
Sodium bicarbonate solution 1 wt.%	2	0
Abex solution 10 wt.%	10	50
Disponil solution 10 wt.%	10	50
Water	142	0

A semicontinuous emulsion polymerization reactor was used in the synthesis. The experimental device consisted of a 1-L glass reactor maintained at 80 °C under nitrogen atmosphere. The reagents corresponding to the main reactor load (shown in Table 1) were introduced to the reactor, except the initiator solution. Once the reactor was maintained at the reaction temperature for 30 min, the initiator solution was added. After 10 min, the addition of the pre-emulsion from the feeding tank started with the aid of a pump. The addition time was 4 h in order to operate under starved-feed conditions and avoid secondary nucleation. After the addition time was over, the latex was maintained at 80 °C for 1 h to reduce the residual monomer and left to cool to ambient temperature. All latexes were neutralized, pH~7, with a concentrated NaOH (J.T. Baker) solution. The solid content in all cases was close to 40 wt.% as designed. A sample of the final polymer dispersion was characterized by quasi-elastic light scattering with a LS Coulter 120 Nanosizer. The average particle size was close to 400 nm in all cases, with a polydispersity index less than 1.01.

To obtain free polymer films for water vapor permeability measurements, cleaned glasses of 10×10 cm^2 were covered with 3 mL of the dispersions and left to dry at laboratory conditions (21 °C and 50% relative humidity) for 5 days. Then, the polymer films were carefully peeled from the glass surface.

In order to measure the water vapor permeability of the films, the procedure described in ASTM E96 [21] was followed, specifically the wet cup test. In this method, a certain amount of water is placed in a glass container which is sealed with the free polymer film. The vials were maintained at laboratory conditions and weighed as a function of time in a balance with 10 mg of error. Each sample was weighed three times and the mean value is reported. For each polymer film, three independent experiments were run.

Film capacitance was determined by Electrochemical Impedance Spectroscopy (EIS), which is a suitable technique to measure the film capacitance without removing the film from the substrate. Low carbon 6×8 cm^2 metal sheets were sanded with paper 600, cleaned, and degreased with acetone; then 2.5 mL of each dispersion was applied and left to dry under ambient conditions for 5 days to give a film thickness around 160 μm with a deviation of 15%. In order to achieve a faster drying rate, the samples were located into a hermetic container with moisture adsorbent for 24 h, and then maintained at ambient conditions for 4 days. The impedance spectra were obtained with a Gill potentiostat, with amplitude of ±10 mV between 10^4 and 10^{-1} Hz using graphite and saturated calomel as auxiliary and reference electrode, respectively. The spectra were obtained after 24 h of continuous immersion in a 0.5 M sodium sulfate solution. Data analysis was carried out by

assuming a R(RC) equivalent circuit at high frequency range using Zview software [22]. The reported points are the mean values of three independent experiments in which the standard deviation does not exceed the symbol size.

Model description

In our previous works [23, 24], a simplified model of the first stage of the film formation process was developed. In those works, the polymer colloid particles were modeled as one-component fluid using the hard-sphere pair potential between the colloids. This simple potential is suitable for describing different colloidal features because it takes into account the excluded volume of the colloids [25–27]; however, surface charge of the colloidal particles as well as the influence of the solvent can be taken into account through an effective pair potential [28, 29], in this way we use the soft spheres potential given by the following equation:

$$\beta U_{cc}(r) = \left(\frac{\sigma}{r}\right)^n \quad (1)$$

where $\beta=k_BT$, k_B and T denote the Boltzmann constant and absolute temperature, respectively, σ is the particle diameter considered as the unit length, r is the distance between particles and n is the softness parameter. It should be noted that the soft potential has a simple form but is able to reproduce the interparticle interaction in real systems. For example, in Fig. 1, a comparison between experimental and simulation results of the two-dimensional radial distribution function, $g(r)$, is shown. The simulations results were obtained by calculating $g(r)$ with a canonical Monte Carlo (MC) simulation using potential (1) with $n=16$. The experimental structure was obtained by Confocal Scanning Laser Microscopy (CSLM) by Dullens et al., taking the images of cross-linked poly(methyl methacrylate) particles suspended in TFH, in the first layer at the bottom glass wall of the sample container [30]. These latex particles behave as soft spheres in THF [31]. As can be seen, there is an excellent agreement between the experimental and simulation structure. The source of the large difference may be the particle size polydispersity of the real system and the resolution of the microscope [32].

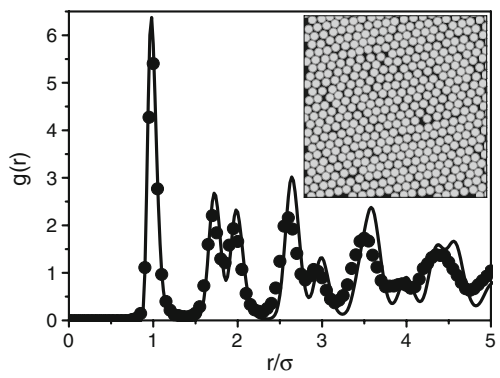

Fig. 1 Comparison of the experimental (*dots*) and simulated (*line*) 2D radial distribution function, *g(r)*. The softness parameter in the simulation is $n=16$. The inset is a snapshot of the simulation results which shows a dense hexagonal packing.

It is interesting to note that $\rho\sigma^2$, where ρ is the two-dimensional number density, i.e., the number of particles divided by the area, is similar in experiment and simulation, 1.082 and 1.136, respectively. The inset in Fig. 1 is a typical simulation configuration of the particles at equilibrium, which can be compared with the experimental picture. In both, a dense hexagonal packing is observed with low defect content. Based on the structure comparison, we assume that potential (1) with n around 16 is appropriate for modeling the *effective* interaction between charged latex particles in water.

Therefore in the present work, the colloidal dispersion is modeled as one-component fluid using the soft spheres pair potential, Eq. (1). The process of drying was simulated as follows. Initially $N=4000$ particles were introduced in a prism of $L_X=L_Y=25\sigma$ and initial length of $L_{Z0}=12.5\sigma$ (see Fig. 2a). The wall located on the left-hand side of Fig. 2a represents the hard impenetrable substrate. Each particle is tested to move m times according to the Metropolis algorithm [33] ($m=16$ for the slow and $m=8$ for the high drying rate), with maximum particle displacement $l_p=0.05$ before the side L_Z reduces by $l_i=0.01\sigma$. This mimics the evaporation of water and the consequent increment of the film density. The influence of the vapor–liquid interfacial tension is modeled using a soft repulsive potential (Eq. (1), with $n_i=8$) between colloidal particles and the right-hand wall; thus, colloidal particles can not leave the continuous phase. Once a particle has been reached by the interface (i.e., it acquires a particle–interphase repulsion larger than 100) it no longer experiments random motion because it is considered to be out of the continuous phase. Such *trick* reproduces the observed phenomena where a porous layer is formed at the vapor–liquid interphase as drying proceeds. The simulation ends when all particles cannot move or $L_Z=0$. The entire evaporation process simulations and the characterization of the simulated films were repeated no less than three times to report the average. A detailed description of the model and the meaning of each parameter can be found elsewhere [23, 24, 34].

It is important to emphasize that the proposed model describes the first stage of the latex film formation, i.e., the particle packing during evaporation. At high densities, the simulated soft particles may partially penetrate each other, which can be considered as deformation and coalescence of the latex particles while the film formation goes on, as seen in Fig. 2b. The resulting film structure consists of hydrophobic cores surrounded by hydrophilic domains [35, 36], denominated cellular films.

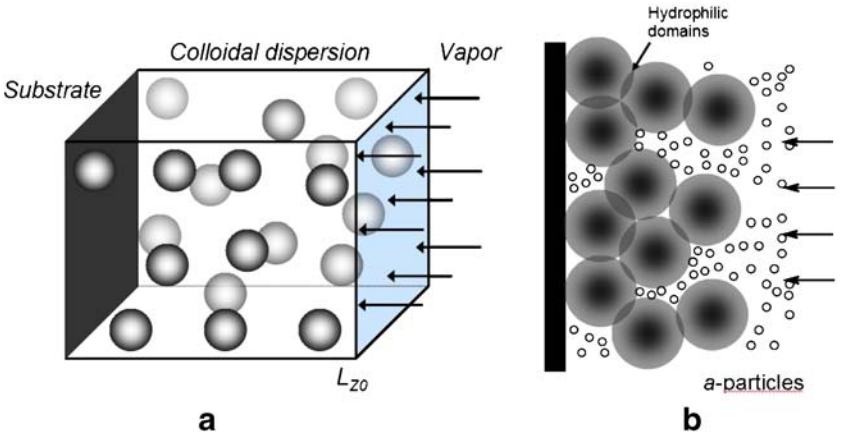

Fig. 2 **a** Schematic representation of the simulation cell. The substrate is located on the left-hand wall. The liquid–vapor interface of the colloidal dispersion moves as depicted by the arrows to simulate the water evaporation. **b** Representation of the final film structure and the algorithm developed to determine the film permeability. a-particles can be located over the surface of colloidal particles because of the soft potential repulsion

In order to evaluate the permeability of the simulated films, N_a=2,000 small *a*-particles ("attacking particles") were placed right next to the film as illustrated in Fig 2b. The pair interaction between these "attacking particles" and dried film particles is given by Eq. (1) with the following parameters $\sigma_{ac}=0.5(\sigma_a+\sigma)$ and $n_{ac}=40$, where σ_a is the diameter of the *a*-particles ($\sigma_a=0.01\sigma$). There is no interaction between *a*-particles; they behave like ideal gas with respect to each other. Such approximation is valid for water vapor permeability we study in the experiment. The *a*-particles were left to diffuse through the film, moving preferentially to the substrate in a ratio of 3:1. In each MC step, we tried to displace all the *a*-particles once. This algorithm was run at least ten times to calculate the average values. The number of MC steps needed for a given number of *a*-particles to reach the substrate will be related to the real time that a given amount of water vapor needs to pass trough the experimental latex film.

The water uptake of the simulated films is determined by locating enough *a*-particles right next to the film to achieve bulk number density $\rho_a=1$. The interaction parameters between these particles and the ones that belong to the film are the same as mentioned above. Among the *a*-particles, only the excluded volume is considered, i.e., they interact through the hard-spheres potential to reflect a dense fluid behavior. This *a*-particle fluid was left to equilibrate and the adsorption isotherm, Γ was calculated using the following equation [26],

$$\Gamma = \int_0^{z_{max}} \rho_a(z)\,\mathrm{d}z \qquad (2)$$

where $\rho_a(z)$ represents the density profile of the *a*-particles and z_{max} is the film thickness calculated from the dried film density profile.

Finally, film surface profiles were calculated according to a recently proposed methodology [34]. Namely, a "probe" ball of diameter 0.025σ was moved perpendicularly to the substrate with a grid space of 0.05, in the *x* and *y* direction. Once the "probe" ball touches a particle of the film surface, the coordinate is saved and employed to generate the film surface profiles and 3D images [37]. This information also can be employed to calculate the roughness of the latex films [38].

Results

The density profiles depicted in Fig. 3 allows us to study the effect of the softness parameter on the internal film structure. Analyzing the layers near the substrate, it is not possible to observe a great difference between the structure of the simulated films, since the broadness and peak height is nearly the same for all systems. One important point to notice is the location of the density peaks: their locations

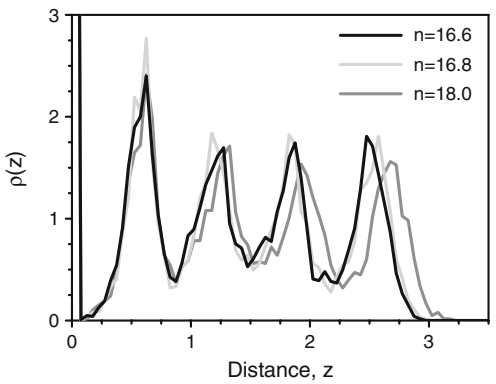

Fig. 3 Density profiles of totally dried films for different softness parameter

suggest a hexagonal array perpendicular to the substrate. However, it should be mentioned that layers close to the air–film interface film surface are reasonably different, over all when n=18. The influence of this small variation on film properties is far from being negligible as will be seen below.

In order to obtain information about the surface topography of the simulated films, in Fig. 4, a series of film surface profiles obtained from our simulations are showed. As we can see, the simulated film with the lowest value of the softness parameter, n=16.6, has quite a flat profile; it means that nearly all the particles lay in the same plane with respect to the substrate, increasing the film surface density and diminishing the defects like channels and cracks. Also, such film may attain low roughness with a consequent high gloss [39]. On the other hand, as the repulsion among the colloidal particles becomes stronger (higher values of n), the roughness of the film increases with the reduction of the barrier properties [34]. The roughness is routinely measured with Atomic Force Microscopy, and it is considered as the standard deviation from the mean value of the height. In Fig. 4, the mean height is presented as a solid line and the standard deviation as a dotted line; it can also be seen that film surface roughness diminishes as the softness parameter becomes lower. As mentioned above, the particle diameter is considered as the unit length, thus RMS values are dimensionless. In case of particles with a diameter of 400 nm employed in this contribution, the difference in film surface roughness would be around 12 nm.

Among several experimental techniques employed to infer the latex film structure, water vapor permeability and gas adsorption offer a nonexpensive and nonlaborious way to correlate some film properties with its structure [40]. Therefore, we have performed a comparison between experimental and simulation results of film permeability. Once the permeation curve (number of a-particles reaching the substrate as a function of MC steps) for n=18 was obtained, we have considered that 500 contacts with the substrate correspond to 0.67 g of water lost and 1,550 MC steps correspond to 16 days of experimental time. Similar relations have been established for the other two latex films. Thus, a linear relation between the number of a-particles that reach the substrate and water lost, as well as between MC steps and elapsed days, has been defined. Both linear relations, shown in Fig. 5, were employed to adjust experimental and simulation permeability results.

The experimental and simulation permeability results are given in Fig. 6. First of all, we would like to highlight that our simulation approach almost perfectly predicts the experimental results. As seen, the lowest permeability is attained by the film with 2 wt.% AA and n=16.6. This film has lower values of permeability due to its compact structure and high density as viewed from the density profiles. The next system, 4 wt.% AA and n=16.8 has a slightly higher permeability. The greatest value of permeability is achieved by the film with 6% AA and n=18. The permeability simulation considers that the vapor transfer is carried out mainly through the (micro)voids left between the colloidal particles and through the hydrophilic domains inside the film. It is considered that the hydrophobic core of the polymer particles does not contribute much to water transport as compared to voids, defects, channels, cracks, and hydrophilic domains of the film [41, 42]. Moreover, since the polymer dispersions were neutralized with NaOH, the polymer chain interdiffusion is retarded, which guarantees that the permeation of water vapor is carried out mainly through interconnected voids and hydrophilic domains [43].

The measurement of the water uptake using EIS is based on the determination of the changes of the coating

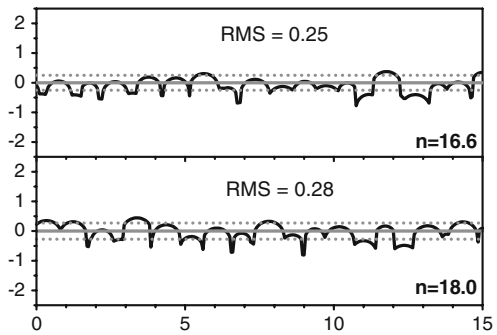

Fig. 4 Two-dimensional profiles of the film surface for different values of n. The film surface roughness is also reported

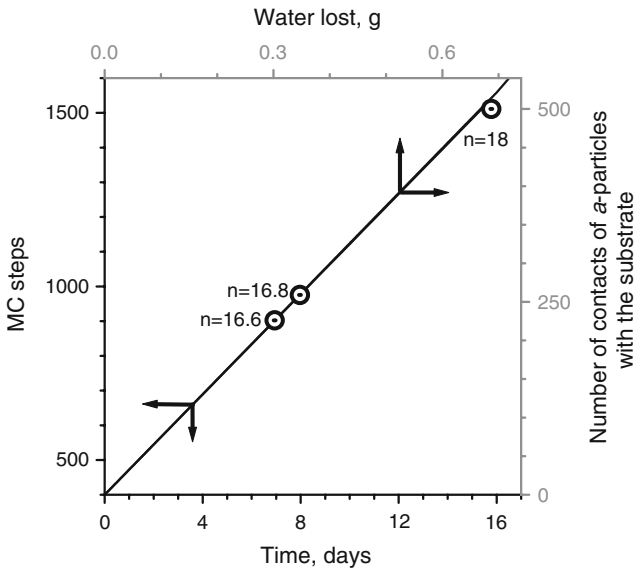

Fig. 5 Linear relation between MC steps and experimental time, as well as particles that reach the substrate and water lost. Points correspond to water lost at 16 days for different acrylic acid content

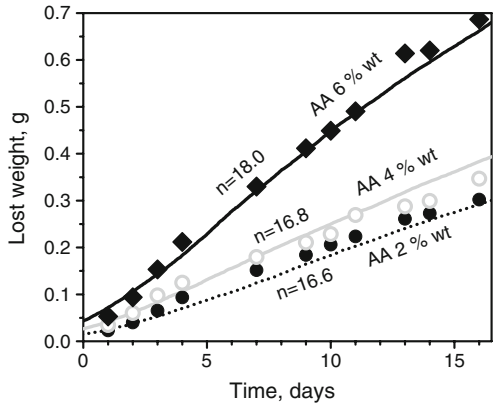

Fig. 6 Experimental and simulation results of the film permeability as a function of time. Points correspond to experimental data and the solid lines are from simulation results

capacitance [44]. The capacitance is directly proportional to the dielectric constant, which for polymeric materials is close to 4–5; meanwhile, for water at 25 °C, it is close to 80. Therefore, any capacitance increment can be related to the presence of water within the film [45]. The measured capacitance of the latex films is showed in Fig. 7. As seen, increasing the AA content in the copolymer enhances the film water uptake. This water uptake increment could be a result of the film morphology because of the AA addition or due to the increment of the hydrophilic nature of the copolymer with the AA addition.

In order to determine which parameter has more influence on the film properties, the change of film structure due to the addition of AA or the modification of the hydrophilic nature of the copolymer, latexes with 2 and 6 wt% AA were dried at a higher drying rate by reducing the humidity of the system, which has a significant influence on the packing of particles. As seen in Fig. 7, at a high drying rate, the capacitance of the film formed with 2 wt.% AA substantially increases, reaching the same value as the film with 6 wt.% AA. More surprising is the fact that the capacitance of the film formed with 6 wt.% AA does not depend on the drying rate. These results allow us to

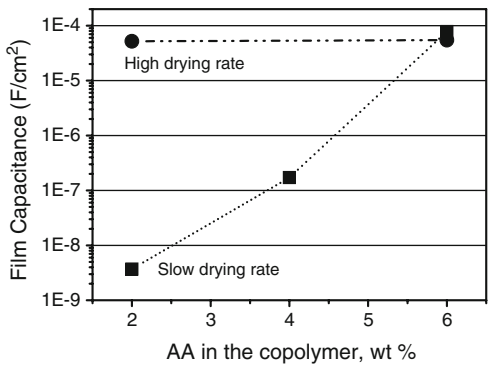

Fig. 7 *Film capacitance* as a function of *AA content*

conclude that the packing of particles has a strong effect on the water uptake by latex films as predicted by our simulation results.

Figure 8a shows the simulation density profiles of the *a*-particles adsorbed into the model colloidal films. In the inner region of the films (close to the substrate), there is no difference in the distribution of the *a*-particles; however, in the layers near the film surface, one can observe that increasing the value of the softness parameter leads to a major presence of adsorbed *a*-particles due to the low-ordered film structure in this region.

The adsorption isotherms in Fig. 8b indicate the amount of *a*-particles that are inside the film, i.e., the integral of the density profiles of Fig. 8a. We can observe that the Γ value increments as the softness parameter augments, which means that as the interparticle repulsion becomes stronger as a result of an increment of surface charge, there is an increment of the film water uptake. This algorithm also considers that adsorbed species are located at the interstices left by the polymer particles and within hydrophilic membranes; therefore, the water uptake is predominantly influenced by the film morphology as a result of the interparticle interaction. In Fig. 8b, it is also shown that by increasing the drying rate, the value of Γ also increases and

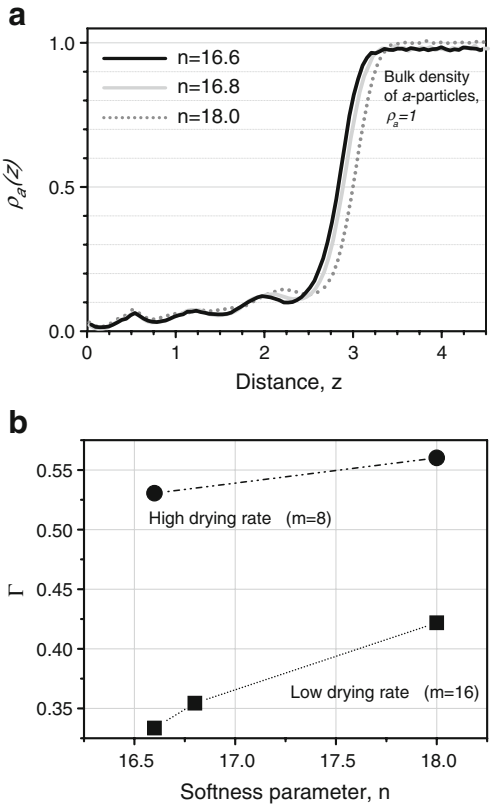

Fig. 8 **a** Density profiles of a-particles inside the colloidal film and **b** adsorption isotherm as a function the softness parameter for different drying rates

there is a minor influence of the softness parameter. Such trend is corroborated by our film capacitance measurements discussed above. Therefore, experimental and simulation results indicate that the influence of the interparticle repulsion on film properties is diminished as the drying rate increases, and the water uptake is affected by the morphology of the film and not only by the addition of hydrophilic monomers.

Conclusions

In this work, the modification of poly(styrene-*co*-butyl acrylate) latex film properties by the addition of acrylic acid is studied with experimental techniques and a simulation approach. It is shown that increasing the colloidal surface charge as a result of the addition of AA leads to latex films with a more porous structure which enhances the passage of water vapor transport and water uptake.

Also, it was demonstrated that films with higher surface roughness exhibit higher water vapor passage and water uptake. In addition, we found that increasing the amount of acrylic acid augments the film water uptake; however in contrast to the common belief, we attribute such results to *both* the hydrophilic nature of the monomer and the latex film structure.

Finally, it is important to mention that the theoretical approach presented in this contribution predicts surprisingly well the water vapor permeability and allows us to analyze the film surface characteristics, which is quite nontrivial to carry out in the case of soft latex particles [46].

Acknowledgements We thank R.P.A. Dullens for kindly supplying his experimental data. Financial support from the Instituto Mexicano del Petróleo (project No. D.31519) is greatly appreciated.

References

1. Sanmiguel M, Soto N, Reyes Y, Vázquez F (2006) Int J Polym Mat 55:595
2. Campos G, Reyes Y, Soto N, Arenas J, Vázquez F (2006) J Reinf Plastics Compos 25:1897
3. Manenosono S, Okubo T, Yamaguchi Y (2003) J Nanopart Res 5:5
4. Li Y, Kunitake T, Fujikawa S (2006) Colloid Surf A 275:209
5. Fitch R (1997) Polymer Colloids: a comprehensive introduction. Academic, San Diego, p 6
6. Musyanovych A, Rossmanith R, Tontsch C, Landfester K (2007) Langmuir 23:5367
7. Koh AYC, Mange S, Bothe M, Leyrer RJ, Gilbert RG (2006) Polymer 47:1559
8. Steward PA, Hearn J, Wilkinson MC (2000) Adv Colloid Interface Sci 86:195
9. Keddie JL (1997) Mat Sci Eng 21:101
10. Winnik MA (1997) In: Lovell PA, El-Aasser MA (eds) Emulsion Polymerization and Emulsion Polymers. Wiley, UK, p 647
11. Belaroui F, Grohens Y, Marie P, Holl Y (2004) Progr. Colloid Polym Sci 128:159
12. Holl Y, Keddie JL, McDonald PJ, Winnik MA (2001) In: Urban M (ed) Film formation in coatings: mechanisms, properties and morphology. ACS symposium series 790. American Chemical Society, Washington, DC, p 2
13. Wang Y, Kats A, Juhué D, Winnik MA (1992) Langmuir 8:1435
14. Rieger J, Hädicke E, Ley G (1992) Phys Rev Lett 68:2782
15. Lallet F, Olivi-Tran N (2006) Phys Rev E 74:061401
16. Castela ASL, Simoes AM, Ferreira MGS (2000) Prog Org Coat 38:1
17. Gundabala VR, Zimmerman WB, Routh AF (2004) Langmuir 20:8721
18. Zohrehvand S, te Nijenhuis K (2005) Colloid Polym Sci 283:305
19. Mohanty PS, Kesavamoorth P, Matsumoto K, Matsuoka H, Venkatesan KA (2006) Langmuir 22:4552
20. Rottstegge J, Kindervater P, Wilhem M, Landfester K, Heldmann C, Fisher JP, Spiess HW (2003) Colloid Polym Sci 281:1111
21. Standard ASTM E96/E 96M-05 (1995) Standard test methods for water vapor transmission of materials. American Society for Testing Materials, Philadelphia
22. Reyes Y, Rodriguez FJ, del Río JM, Corea M, Vázquez F (2005) Prog Org Coat 52:366
23. Reyes Y, Duda Y (2005) Langmuir 21:7057
24. Reyes Y, Vázquez F, Duda Y (2005) Adv in Tech Mat and Mat Proc J 7:127
25. Bryant G, Williams SR, Qian L, Snook IK, Pérez E, Pincet F (2002) Phys Rev E 66:060501
26. Trokhymchuk A, Henderson D, Nikolov A, Wasan DT (2003) J Phys Chem 107:3927
27. Pusey PN, van Megen W, Barttlet P, Ackerson BJ, Rarity JG, Underwood SM (1989) Phys Rev Lett 63:2753
28. Guevara-Rodríguez FD, Medina-Noyola M (2003) Phys Rev E 68:011405
29. Israelachvili JN (1998) Intermolecular and surface forces. Academic, San Diego, p 112
30. Dullens RPA, Claesson EM, Kegel WK (2004) Langmuir 20:658
31. Dullens RPA, Claesson M, Derks D, van Blaadaren A, Kegel WK (2003) Langmiur 19:5963
32. Royall CP, Louis AA, Tanaka H (2007) J Chem Phys 127:044507
33. Landau DP, Binder K (2000) A guide to Monte Carlo simulations in statistical physics. Cambridge University Press, Cambridge, p 48
34. Reyes Y, Campos-Terán J, Vázquez F, Duda Y (2007) Modeling Simul Mater Sci Eng 15:355
35. Rharbi Y, Boué F, Janicot M, Cabane B (1996) Macromolecules 29:4346
36. Kim HB, Winnik MA (1994) Macromolecules 27:1007
37. Bogana M, Donadio D, Benedek G, Colombo L (2001) Europhys Lett 54:72
38. Pérez E, Lang J (2000) Langmuir 16:1874
39. Otts DB, Cueva-Parra LA, Pandey RB, Urban MW (2005) Langmuir 21:4034
40. Carbajo MC, Climent E, Enciso E, Torralvo MJ (2005) J Colloid Interface Sci 284:639
41. Aramendia E, Barandiaran MJ, Grade J, Blease T, Asúa JM (2005) Langmuir 21:1428
42. Agarwal N, Farris RJ (1999) J Appl Polym Sci 72:1407
43. Kim HB, Winnik MA (1995) Macromolecules 28:2033
44. Lui C, Bi Q, Leyland A, Matthews A (2003) Corrosion Sci 45:1243
45. Deflorian F, Fredizzi L, Rossi S, Bonora PL (1999) Electrochem Acta 44:4243
46. Mallégol J, Dupont O, Keddie JL (2001) Langmuir 17:7022